Scientific Research Publishing

Energy and Power Engineering, 2023, 15, 340-352
https://www.scirp.org/journal/epe
ISSN Online: 1947-3818
ISSN Print: 1949-243X

Analysis of Light Load Efficiency Characteristics of a Dual Active Bridge Converter Using Wide Band-Gap Devices

Bongwoo Kwak

Automotive Materials & Components R & D Group, Korea Institute of Industrial Technology, Gwangju, Korea
Email: bwkwak11@kitech.re.kr

How to cite this paper: Kwak, B. (2023) Analysis of Light Load Efficiency Characteristics of a Dual Active Bridge Converter Using Wide Band-Gap Devices. *Energy and Power Engineering*, **15**, 340-352.
https://doi.org/10.4236/epe.2023.1510019

Received: September 15, 2023
Accepted: October 20, 2023
Published: October 23, 2023

Abstract

In this paper, the zero voltage switching (ZVS) region of a dual active bridge (DAB) converter with wide band-gap (WBG) power semiconductor device is analyzed. The ZVS region of a DAB converter varies depending on output power and voltage ratio. The DAB converters operate with hard switching at light loads, it is difficult to achieve high efficiency. Fortunately, WBG power semiconductor devices have excellent hard switching characteristics and can increase efficiency compared to silicon (Si) devices. In particular, WBG devices can achieve ZVS at low load currents due to their low parasitic output capacitance ($C_{o,tr}$) characteristics. Therefore, in this paper, the ZVS operating resion is analyzed based on the characteristics of Si, silicon carbide (SiC) and gallium nitride (GaN). Power semiconductor devices. WBG devices with low $C_{o,tr}$ operate at ZVS at lower load currents compared to Si devices. To verify this, experiments are conducted and the results are analyzed using a 3 kW DAB converter. For Si devices, ZVS is achieved above 1.4 kW. For WBG devices, ZVS is achieved at 700 W. Due to the ZVS conditions depending on the switching device, the DAB converter using Si devices achieves a power conversion efficiency of 91% at 1.1 kW output. On the other hand, in the case of WBG devices, power conversion efficiency of more than 98% is achieved under 11 kW conditions. In conclusion, it is confirmed that the WBG device operates in ZVS at a lower load compared to the Si device, which is advantageous in increasing light load efficiency.

Keywords

Dual Active Bridge (DAB) Converter, Zero Voltage Switching (ZVS), ZVS Region, Wide Band-Gap Power Semiconductor, Parasitic Output Capacitance

1. Introduction

Recently, renewable energy has been widely used due to the depletion of fossil fuels and the need to reduce carbon dioxide. In particular, research on energy storage system (ESS) that uses batteries is being actively conducted for the efficient operation of renewable energy using solar and wind power [1]. Additionally, interest in DC power distribution is increasing. DC distribution has many advantages over AC distribution because transmission losses due to AC resistance and power conversion steps are reduced [2]. **Figure 1** shows the DC microgrid configuration. A bidirectional power conversion system is essential to efficiently control the power of a DC microgrid using ESS [3] [4].

Dual Active Bridge (DAB) is widely used as an isolated bidirectional converter for DC microgrid. The DAB converter is a full bridge circuit with the same primary and secondary sides, enabling bidirectional power transfer through phase control on both ends of the transformer. When the primary and secondary sides of a DAB converter have the same voltage ratio, zero voltage switching (ZVS) is possible over a wide load range, increasing efficiency. However, in the case of batteries, the voltage varies depending on the state of charge (SOC), and it is difficult to implement ZVS under light load conditions when connected directly to the DAB converter [5] [6] [7].

Typically, DAB converters have a two-stage structure that includes a non-isolated converter for charging and discharging the battery to maintain a constant voltage ratio. However, the two-stage configuration has limitations in increasing efficiency and power density. As a result, the DAB converter must be connected directly to the battery to achieve high power density and efficiency [8] [9]. However, hard switching occurs at light load depending on the changing voltage ratio. In particular, silicon (Si) power semiconductor devices, which are widely used in power conversion systems, are significantly less efficient in hard switching due to physical limitations [10].

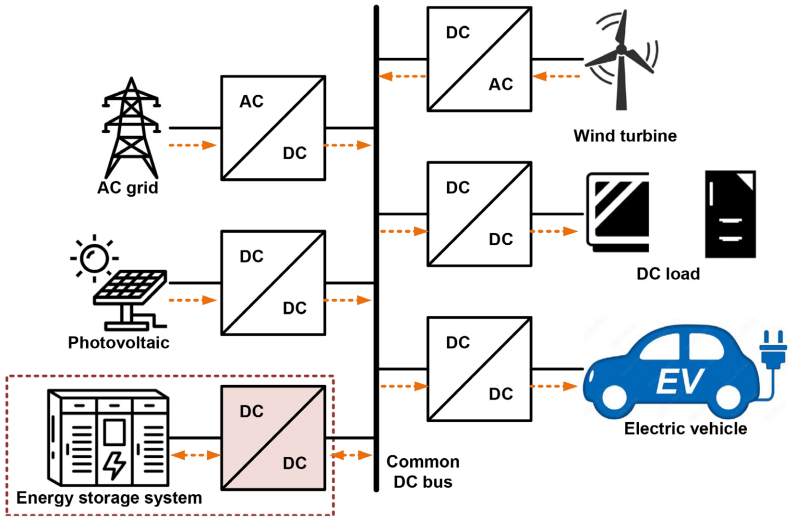

Figure 1. Structure of DC microgird.

To improve the hard switching problem, various switching techniques have been applied in [11] [12] to achieve a wide range of ZVS. ZVS is achieved over a wide load range through switching technology, improving light load efficiency. In [13], a dual transformer is applied to implement a wide range of ZVS. The above methods apply complex control algorithms or require additional hardware to achieve light load ZVS. ZVS implementation at lower loads is an important issue in the topology of the DAB converter. Therefore, an analytical approach is needed to achieve ZVS at lower loads without additional hardware.

Recently, wide bandgap (WBG) devices are widely used as an alternative to overcome the physical characteristics of Si devices. Representative WBG devices include silicon carbide (SiC) and gallium nitride (GaN). WBG devices are capable of fast switching due to their high bandgap energy, high saturation electron velocity, and electron mobility properties [14] [15]. In addition, it has a high thermal conductivity, making it advantageous at high temperatures, and has a lower on resistance ($R_{ds,on}$) than Si at the same breakdown voltage due to its excellent specific on-resistance (RSP) characteristics [16]. In particular, WBG devices can accelerate drain-source transitions during switching due to their low parasitic output capacitance ($C_{o,tr}$) characteristics, resulting in ZVS at lower load currents [17].

In this paper, the ZVS characteristics are analyzed under light load conditions when a WBG device is applied to a DAB converter whose ZVS region varies depending on the load conditions. In addition, efficiency characteristics under light load conditions are compared through DAB converter experiments using Si and WBG devices.

2. Dual Active Bridge Converter for ESS

2.1. Circuit Configuration and Operating Principle for DAB Converter

Figure 2 shows the circuit of a DAB converter. The DAB converter consists of a full bridge circuit with the same primary and secondary sides, and an external inductor and transformer are connected in series.

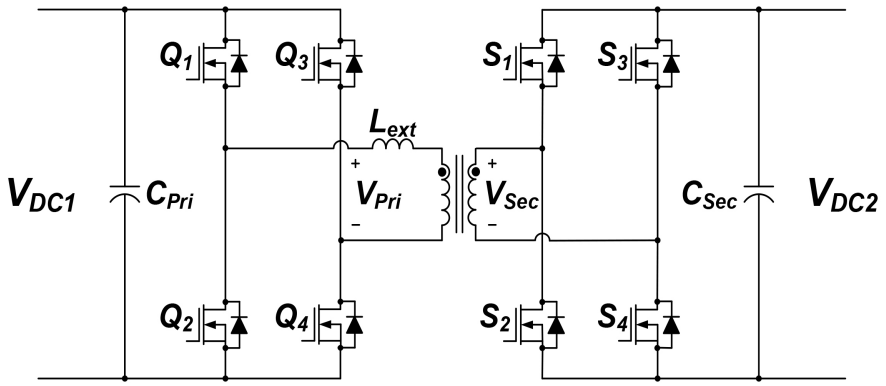

Figure 2. Schematic of dual active bridge converter for ESS.

The output power of the DAB converter is determined by the inductance of the external inductance, as shown in Equation (1). The inductance should be selected considering the maximum output [18] [19].

$$P_{OUT} = \frac{nV_{DC1}V_{DC2}D(1-D)}{2f_{sw}L_{ext}}. \quad (1)$$

where, f_{sw} is the switching frequency, n is the transformer turns ratio, and D is the phase difference (radians/π), which must be less than 0.5.

2.2. ZVS Analysis of DAB Converter

In DAB converters, ZVS is determined by the external inductor current. Therefore, analysis of the external inductor current is important. **Figure 3** shows the external inductor current waveform over one cycle, and the equations for I_{L1} and I_{L2} of the current are as Equation (2) and Equation (3) [20].

$$I_{L1} = -\frac{V_{DC1}}{4f_{sw}L_{ext}} - \frac{nV_{DC2}(2D-1)}{4f_{sw}L_{ext}}. \quad (2)$$

$$I_{L2} = \frac{nV_{DC2}}{4f_{sw}L_{ext}} + \frac{V_{DC1}(2D-1)}{4f_{sw}L_{ext}}. \quad (3)$$

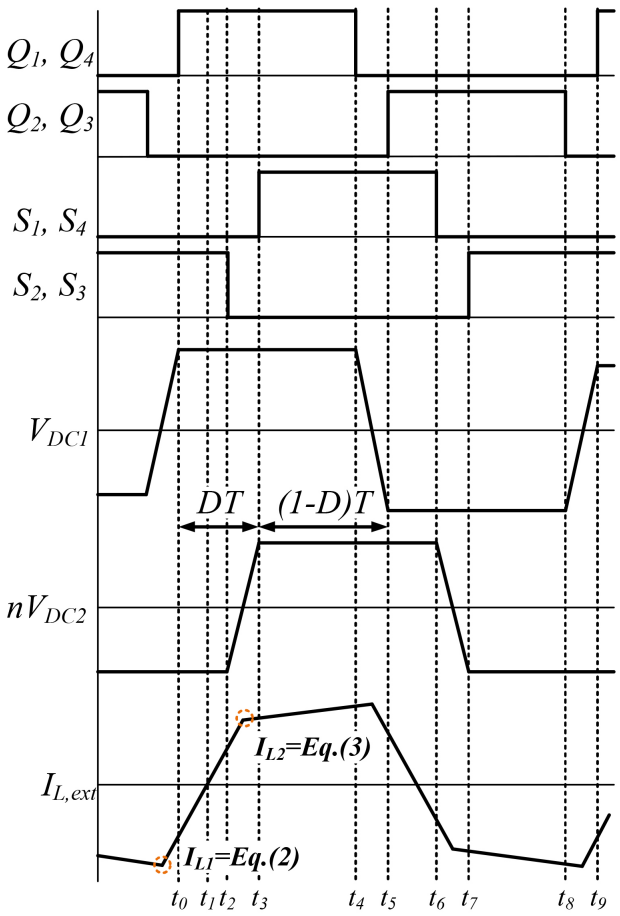

Figure 3. Key waveforms of DAB converter.

Based on Equations (2) and Equations (3), the ZVS condition varies depending on the input/output voltage ratio. Table 1 shows the ZVS conditions for the primary and secondary full bridge legs as a function of voltage ratio. Where, M is the primary to secondary voltage ratio. When a DAB converter is applied to a battery system application, the ZVS conditions vary depending on the SOC. When the load current exceeds a certain level, the entire area is operated at ZVS, so the influence of ZVS is significant under light load conditions.

The ZVS is achieved only when the energy stored in the parasitic output capacitance is fully charged and discharged during the turn-off period including the dead time. Therefore, it is necessary to analyze ZVS characteristics considering the effect of $C_{o,tr}$ of the switching element. Figure 4 shows the current flow in the dead time ($t_2 - t_3$) section, and Figure 5 shows the equivalent circuit of the bridge circuit when S_2 and S_3 are turn-off.

In the equivalent circuit, the parasitic capacitance current can be defined by Equation (4) and the external inductor current can be defined by Equation (5).

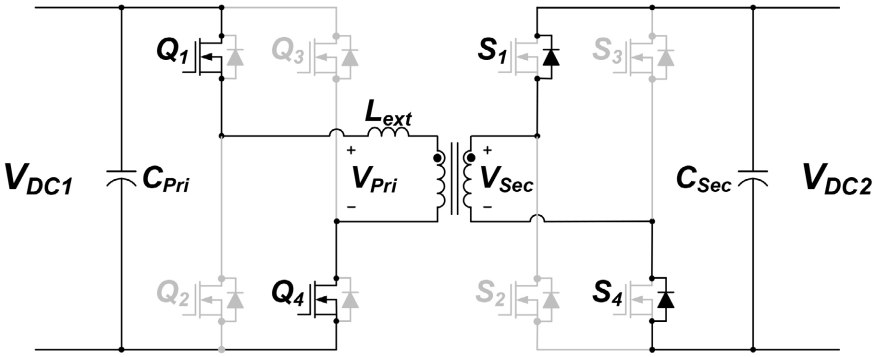

Figure 4. Power flow in the DAB converter during t_2 - t_3.

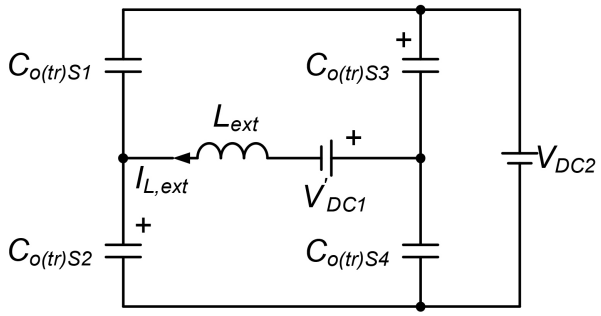

Figure 5. Equivalent circuit of full bridge when S_2 and S_3 are turned off.

Table 1. The ZVS conditions based on the voltage ratio.

Condition	1st side	2nd side
$M = 1$	ZVS	ZVS
$M > 1$	$I_{L1} < 0$	ZVS
$M < 1$	ZVS	$I_{L2} > 0$

$$I_{Co(tr)} = C_{o(tr)} \frac{DV_{Co(tr)}}{dt}. \tag{4}$$

$$I_{L,ext} = 2C_{o(tr)} \frac{DV_{Co(tr)}}{dt}. \tag{5}$$

As a result, the current required for ZVS is defined by the equation:

$$L_{ext} I_{L,ext}^2 = EC_{o(tr)}.$$

$$\frac{1}{2} L_{ext} I_{L,ext}^2 = 2C_{o(tr)} V'_{DC1} V_{DC2}.$$

$$I_{L,ext} = 2\sqrt{\frac{C_{o(tr)} V'_{DC1} V_{DC2}}{L_{ext}}}. \tag{6}$$

Through the above equation, the $C_{o,tr}$ of the power semiconductor device must be considered to accurately calculate the ZVS area of the DAB converter.

In this paper, Si, SiC, and GaN devices are compared and analyzed to analyze the ZVS area of the DAB converter due to the parasitic components of the switching device. The power semiconductor devices selected are IPW65R035CFD7 (Si MOSFET, Infineon), IMW65R030M1HXKSA1 (SiC MOSFET, Infineon), and TP65H035G4WS (GaN FET, Transphorm). Devices with similar $R_{DS,on}$ resistance characteristics were selected. All use the same TO-247 package. Key specifications are listed in Table 2.

Figure 6 shows the calculated ZVS region considering the $C_{o,tr}$ of each switching device. It can be seen that the larger the $C_{o,tr}$, the higher the load conditions required to achieve ZVS. Therefore, since the $C_{o,tr}$ of the WBG device is lower than that of the Si device, ZVS can be achieved under light load conditions.

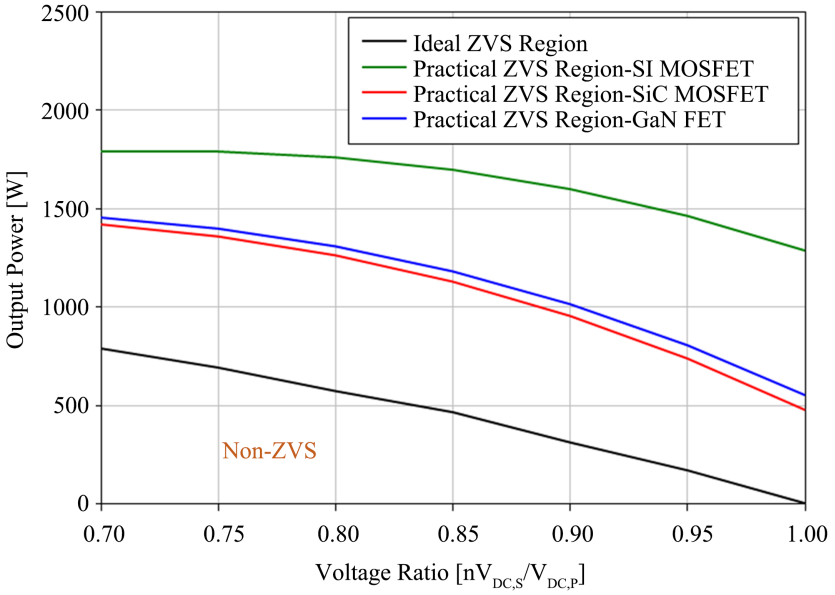

Figure 6. ZVS boundary comparison for practical conditions by power semiconductor devices.

Table 2. Key specifications by power semiconductor device.

Parameter	Si MOSFET	SiC MOSFET	GaN FET
$R_{DS,on}$	29 mΩ	30 mΩ	35 mΩ
C_{iss}	7149	18 pF	1500 pF
$C_{o,tr}$	2427 pF	284 pF	380 pF
Q_g	145 nC	48 nC	22 nC

3. Experimental Results and Discussion

The ZVS characteristics according to power semiconductor devices were verified in a 3 kW DAB converter. Figure 7 shows a prototype of a 3 kW DAB converter. The gate driver used Skyworks' si823H9. In addition, a similar PCB pattern was applied to minimize the effect of parasitic inductance when driving the gate of Si, SiC, and GaN power semiconductor devices. Figure 8 shows the gate pattern between the gate driver and switching device that is actually used. The DAB converter is controlled using a digital controller based on TMS320F280049C (Texas Instruments Inc.). The design specifications and experimental conditions of the DAB converter are shown in Table 3. External inductor is calculated based on output power and switching frequency, it is the sum of the leakage inductance and the inductance of the inductor. Figure 9 shows the overall experimental environment.

Figure 10 shows the ZVS waveforms for each switching device. When Si MOSFETs are used, ZVS is achieved at an output of 1.4 kW. On the other hand, SiC MOSFET is implemented at 700 W, and GaN FET is implemented at 600 W. The low $C_{o,tr}$ characteristic of the WBG device achieved ZVS under a light-load condition therefore, it is advantageous to achieve high efficiency when applied to a converter.

Figure 11 shows the forward experiment results of the DAB converter using GaN FET. The control method is a single-phase shift method, and it is confirmed that the phase increases as the output increases.

Figure 12 shows the efficiency characteristics of the DAB converter with each power semiconductor device applied. Efficiency is low at light loads due to conduction losses due to circulating current and switching losses due to hard switching. However, WBG devices have excellent dv/dt and di/dt characteristics and have low switching losses during hard switching. In addition, it is confirmed that the efficiency is higher than Si devices due to low gate loss due to low Q_g. The efficiency of the DAB converter using Si MOSFET is high under load conditions operating at ZVS. This is because $R_{DS,on}$ is relatively smaller, resulting in lower conduction loss. If $R_{DS,on}$ is the same, the WBG device can achieve higher efficiency under full load conditions.

As a result, ZVS is achieved at lower loads due to the low $C_{o,tr}$ characteristics of the WBG device, and the experimental results show that the efficiency is improved by about 7% compared to Si under 1.1 kW light load conditions.

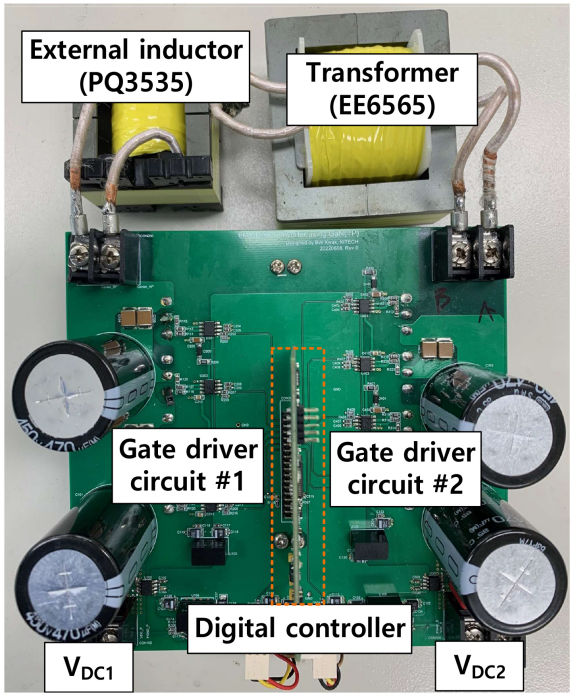

Figure 7. Prototype of 3 kW class DAB converter.

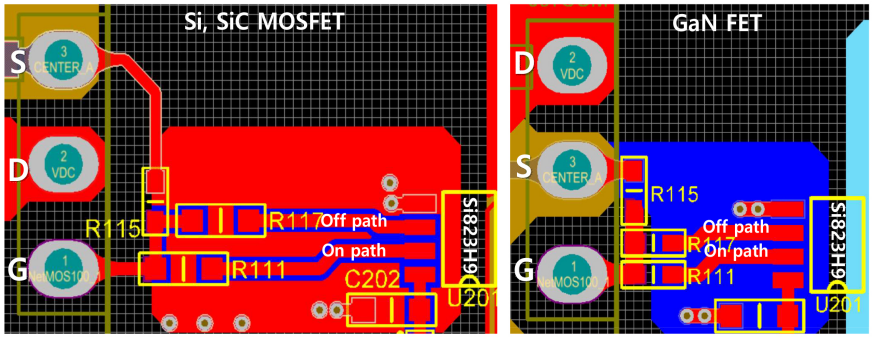

Figure 8. Gate signal pattern for each power semiconductor device.

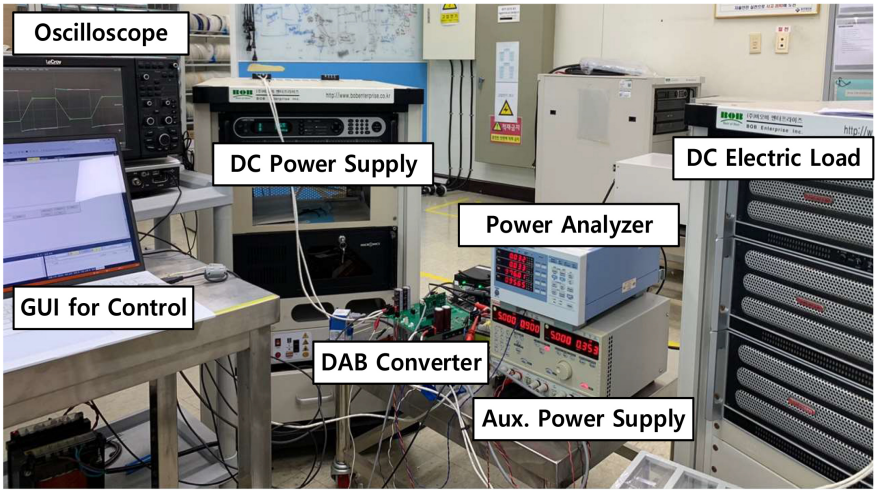

Figure 9. Experimental setup of DAB converter.

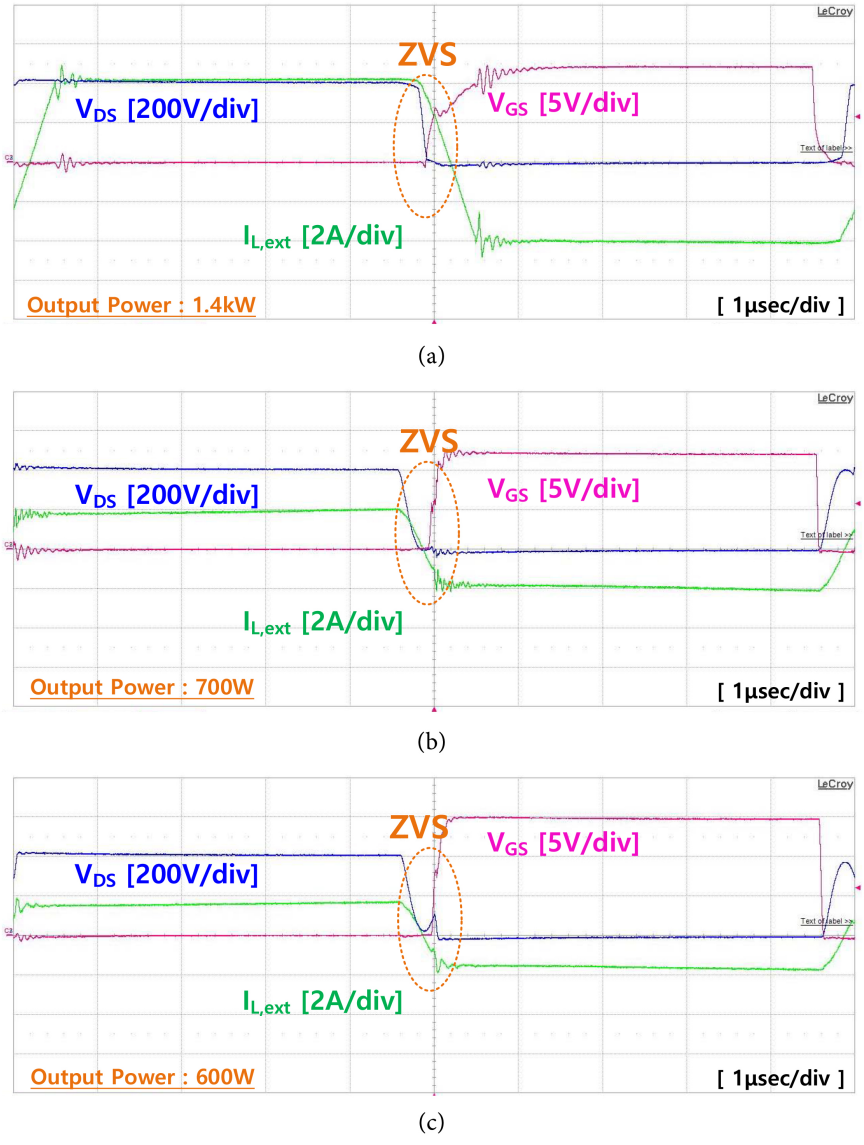

Figure 10. ZVS waveform and load conditions for each power semiconductor device. (a) Si MOSFET; (b) SiC MOSFET; (c) GaN FET.

Table 3. Specifications of DAB converter.

V_{DC1}, V_{DC2}	400 V	P_{OUT}	3 kW
C_{Pri}, C_{Sec}	540 μF	f_{sw}	100 kHz
L_{ext}	60 μH	Dead time	400 nsec
L_m	600 μH	Turn ratio	1:1

Application of WBG devices to topologies with partial ZVS characteristics, such as DAB converters, can achieve high efficiency and high power density. Considering the withstand voltage characteristics of WBG devices, GaN power semiconductor devices are suitable for applications below 600 V, and SiC power semiconductor devices are suitable for applications above 600 V.

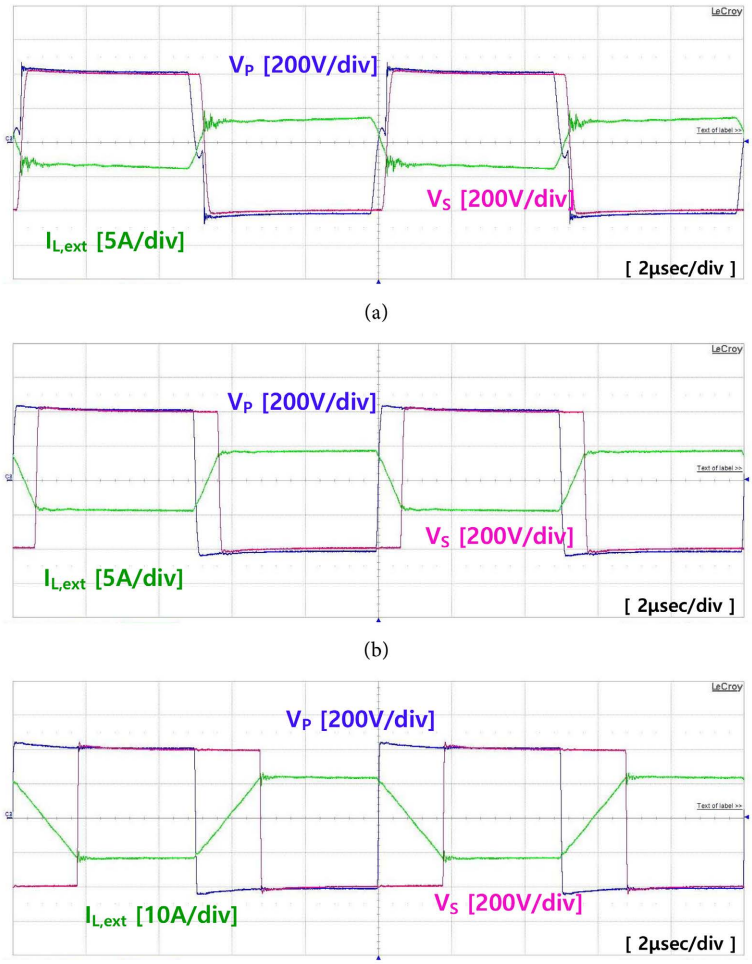

Figure 11. Steady-state waveforms of DAB converter using GaN FET. (a) 500 W; (b) 1500 W; (c) 3000 W.

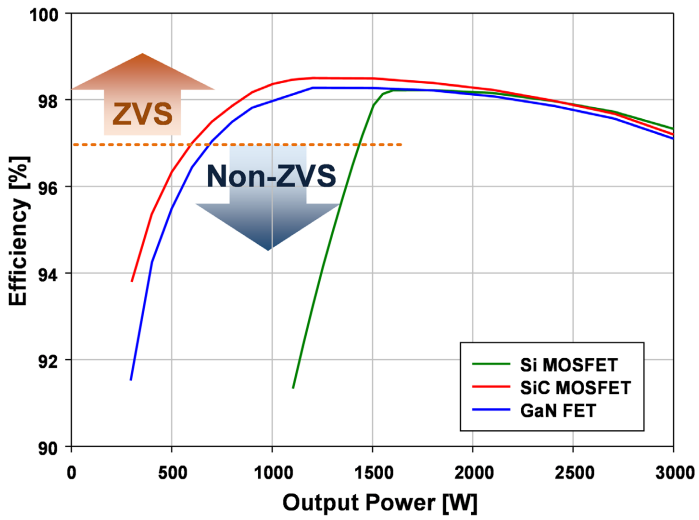

Figure 12. Efficiency characteristics according to the load of each power semiconductor device.

4. Conclusion

In this paper, the ZVS region of a DAB converter using WBG power semiconductor devices is analyzed. WBG power semiconductor devices have excellent hard switching characteristics and can increase efficiency compared to Si devices. In particular, WBG devices can achieve ZVS at low load currents due to their low $C_{o,tr}$ characteristics. Therefore, in this paper, the ZVS operating area is analyzed and verified based on the characteristics of Si, SiC, and GaN. WBG devices with low $C_{o,tr}$ achieve ZVS at lower load currents compared to Si devices. To verify this, an experiment is conducted using a 3 kW DAB converter and the results are analyzed. By applying Si devices, ZVS is achieved at 1.4 kW output condition. On the other hand, WBG devices achieved ZVS at 700 W or less. This confirms that it is advantageous to achieve high efficiency at light loads due to the excellent high-speed switching characteristics of the WBG device and the fast ZVS achieved. Therefore, due to the withstand voltage characteristics of the WBG device, it can be seen that GaN devices are a good choice for applications below 600 V, and SiC devices are a good choice for applications above 600 V.

In future research, charge/discharge experiments will be performed by linking the battery system to WBG and Si-based DAB converters. The excellence of the WBG device is proven through analysis of efficiency data in the constant voltage section with low current, and the battery energy use efficiency is additionally analyzed.

Acknowledgements

This work was supported by the Technology Innovation Program (or Industrial Strategic Technology Development Program-Next-generation power semiconductor technology development project based on compound materials) (RS-2022-00144490, Development of Highly Efficient and Intelligent Solar Energy Harvesting System integrating 600 V level GaN Device funded By the Ministry of Trade, Industry & Energy (MOTIE, Korea).

Conflicts of Interest

The author declares no conflicts of interest regarding the publication of this paper.

References

[1] Tushar, M.H.K., Zeineddine, A.W. and Assi, C. (2018) Demand-Side Management by Regulating Charging and Discharging of the EV, ESS, and Utilizing Renewable Energy. *IEEE Transactions on Industrial Informatics*, **14**, 117-126. http://doi.org/10.1109/TII.2017.2755465

[2] Lotfi, H. and Khodaei, A. (2017) AC versus DC Microgrid Planning. *IEEE Transactions on Smart Grid*, **8**, 296-304. https://doi.org/10.1109/tsg.2015.2457910

[3] Xu, Q., Vafamand, N., Chen, L., Dragičević, T., Xie, L. and Blaabjerg, F. (2021) Review on Advanced Control Technologies for Bidirectional DC/DC Converters in DC Microgrids. *IEEE Journal of Emerging and Selected Topics in Power Electronics*, **9**, 1205-1221. https://doi.org/10.1109/jestpe.2020.2978064

[4] Hill, C.A., Such, M.C., Chen, D., Gonzalez, J. and Grady, W.M. (2012) Battery Energy Storage for Enabling Integration of Distributed Solar Power Generation. *IEEE Transactions on Smart Grid*, **3**, 850-857. https://doi.org/10.1109/TSG.2012.2190113

[5] Yuan, J., Dorn Gomba, L., Callegaro, A.D., Reimers, J. and Emadi, A. (2021) A Review of Bidirectional On Board Chargers for Electric Vehicles. *IEEE Access*, **9**, 51501-51518. https://doi.org/10.1109/ACCESS.2021.3069448

[6] Siebke, K. and Mallwitz, R. (2020) Comparison of a Dual Active Bridge and CLLC Converter for On Board Vehicle Chargers Using GaN and Time Domain Modeling Method. 2020 *IEEE Energy Conversion Congress and Exposition* (*ECCE*), Detroit, 11-15 October 2020, 1210-1216. https://doi.org/10.1109/ECCE44975.2020.9236260

[7] Assadi, S.A., Matsumoto, H., Moshirvaziri, M., Nasr, M., Zaman, M.S. and Trescases, O. (2020) Active Saturation Mitigation in High Density Dual Active Bridge DCDC Converter for on Board EV Charger Applications. *IEEE Transactions on Power Electronics*, **35**, 4376-4387. https://doi.org/10.1109/TPEL.2019.2939301

[8] Wang, H., Yan, K., Ling, Z., *et al.* (2017) Switching Strategy for Isolated Dual Active-Bridge Converter. *IET Power Electron*, **10**, 29-37. https://doi.org/10.1049/iet-pel.2015.0916

[9] Corradini, L., Seltzer, D., Bloomquist, D., *et al.* (2014) Zero Voltage Switching Technique for Bidirectional dc/dc Converters. *IEEE Transactions on Power Electronics*, **29**, 1585-1594. https://doi.org/10.1109/TPEL.2013.2265019

[10] Millan, J. (2014) Survey of Wide Bandgap Power Semiconductor Devices. *IEEE Transactions on Power Electronics*, **29**, 2155-2163. https://doi.org/10.1109/TPEL.2013.2268900

[11] Dung, N.A., Chiu, H.J., Lin, J.Y., Hsieh, Y.C. and Liu, Y.C. (2018) Efficiency Optimisation of ZVS Isolated Bidirectional DAB Converters. *IET Power Electronics*, **11**, 1499-1506. https://doi.org/10.1049/iet-pel.2017.0723

[12] Oggier, G., García, G.O. and Oliva, A.R. (2011) Modulation Strategy to Operate the Dual Active Bridge DC-DC Converter under Soft Switching in the Whole Operating Range. *IEEE Transactions on Power Electronics*, **26**, 1228-1236. https://doi.org/10.1109/TPEL.2010.2072966

[13] Xu, G., Sha, D., Xu, Y. and Liao, X. (2018) Dual-Transformer-Based DAB Converter with Wide ZVS Range for Wide Voltage Conversion Gain Application. *IEEE Transactions on Industrial Electronics*, **65**, 3306-3316. https://doi.org/10.1109/TIE.2017.2756601

[14] Mishra, U.K., Shen, L., Kazior, T.E. and Wu, Y.F. (2008) GaN Based RF Power Devices and Amplifiers. *Proceedings of the IEEE*, **96**, 287-305. https://doi.org/10.1109/JPROC.2007.911060

[15] Yadlapalli, R.T., Kotapati, A., Kandipati, R., Balusu, S.R. and Koritala, C.S. (2021) Advancements in Energy Efficient GaN Power Devices and Power Modules for Electric Vehicle Applications: A Review. *International Journal of Energy Research*, **45**, 12638-12664. https://doi.org/10.1002/er.6683

[16] Dimitrijev, S., Han, J., Moghadam, H.A. and Aminbeidokhti, A. (2015) Power Switching Applications beyond Silicon: Status and Future Prospects of SiC and GaN Devices. *MRS Bulletin*, **40**, 399-405. https://doi.org/10.1557/mrs.2015.89

[17] Jafari, A., *et al.* (2020) Comparison of Wide-Band-Gap Technologies for Soft-Switching Losses at High Frequencies. *IEEE Transactions on Power Electronics*, **35**, 12595-12600. https://doi.org/10.1109/TPEL.2020.2990628

[18] He, P. and Khaligh, A. (2017) Comprehensive Analyses and Comparison of 1 KW Isolated DC-DC Converters for Bidirectional EV Charging Systems. *IEEE Transactions on Transportation Electrification*, **3**, 147-156. https://doi.org/10.1109/TTE.2016.2630927

[19] Yilmaz, M. and Krein, P.T. (2013) Review of Battery Charger Topologies, Charging Power Levels, and Infrastructure for Plug-In Electric and Hybrid Vehicles. *IEEE Transactions on Power Electronics*, **28**, 2151-2169. https://doi.org/10.1109/TPEL.2012.2212917

[20] Choi, H.J. and Jung, J.H. (2016) Practical Design of Dual Active Bridge Converter as Isolated Bi-Directional Power Interface for Solid State Transformer Applications. *Journal of Electrical Engineering & Technology*, **11**, 1265-1273. https://doi.org/10.5370/JEET.2016.11.5.1265